J. Electrical Systems 20-2 (2024): 1426-1435

[1*]Fatma M. Mahmoud,

[2]Amira Nabil,

[3]Mohamed Abouelatta,

[1]Gamal M. Dousoky,

[1,4]M. A. Abdelghany

GaN-HEMT Performance Enhancement

Abstract: - In this work, a simulation analysis and calibration are carried out to improve the performance of AlGaN/GaN- MOSHEMTs (Metal-Oxide Semiconductor High Electron Mobility Transistors). The effect of the AlGaN layer thickness, gate length, Al mole fraction, and the interface traps on the electrical performance of the device has been presented. Device simulations have been done using Sentaurus technology computer-aided design (TCAD). The simulations and analysis show better drain current, transconductance, and cut-off frequency performance. The maximum cut-off frequency shown by the proposed HEMT device is 45.7 GHz at 100-nm gate length. Good transcoductance has been obtained by scaling down the gate length of the device, which is ascribed to the present two-dimensional electron gas (2DEG) density that supports upgrading the output current. Higher drain current is achieved without using acceptor-like traps in the Al_2O_3/AlGaN interface. Results show that the Al_2O_3/AlGaN/GaN-based MOSHEMT is a promising device for high-frequency and power electronic applications.

Keywords: GaN, MOSHEMT, Cut-Off frequency.

I. INTRODUCTION

Owing to their intrinsic features, Group III-nitride semiconductors such as GaN have captured the interest of industries as attractive compounds for optoelectronic, high- power, and high-frequency applications due to their inherent characteristics. Multiple semiconductor materials (e.g., GaN, GaAs, and SiC) have also been proven to be superior to silicon in radio-frequency (RF) and microwave applications [1-3].

GaN/AlGaN heterostructure devices are used in high-power microwave applications. The large bandgap offset at the AlGaN/GaN interface and the charges due to spontaneous and piezoelectric polarization of AlGaN/GaN at the interface provide high carrier mobility in the channel, when fast electronic applications are needed [4].

On the other hand, arsenide- and phosphide-based semiconductors as III–V compound semiconductors are utilized in high-power electronic devices. However, GaN has proven to be a good material for general electronic applications that require high temperature, high-power and high-frequency owing to its superior performance and electron-transport properties. Table I compares the several features of Silicon, GaAs,4H-SiC, and GaN. GaN is acknowledged as one of the most competitive technologies for many applications, according to the combined figure of merit (CFOM) [5].

Table I: Semiconductor-material parameter comparison at 300 K [6].

Feature	Si	GaAs	4H-SiC	GaN
Bandgap Eg (eV)	1.12	1.42	3.25	3.40
Critical Breakdown Field E_B (10^6 V/cm)	0.25	0.4	3.0	4.0
Mobility of electron μ (cm^2/V s)	1350	6000	800	1300
Peak sat. velocity v_s (10^7cm/s)	1.0	2.0	2.0	3.0
Thermal conductivity χ (W/cm K)	1.5	0.5	4.9	1.3

[1]*Corresponding author: Electrical Engineering Department, Faculty of Engineering, Minia University, Minia 61517, Egypt; E-mail: eng.fatima2012@yahoo.com.

[2]Department of Electronics and Electrical Communications, Higher Institute for Engineering and Technology, 5th Settlement, New Cairo, Egypt;

[3] Department of Electronics and Electrical Communications, Faculty of Engineering, Ain Shams University, Cairo 11517, Egypt.

[4]Department of Electrical Engineering, College of Engineering, Prince Sattam Bin Abdulaziz University, Wadi Addwasir 11991, Saudi Arabia.

Copyright © JES 2024 on-line: journal.esrgroups.org

Dielectric constant ε	11.8	12.8	9.7	9.0
CFOM 1 = $(\chi\varepsilon\mu v_s {E_B}^2)/(\chi\varepsilon\mu v_s {E_B}^2)_{Si}$	1	8	458	489

1 CFOM for high temperature/high-power/high-frequency applications.

The bandgap of GaN is 3.4 eV, the peak saturation velocity (v_s) of 3×10^7 $cm\cdot s^{-1}$ at the room temperature, a critical breakdown field of 4 $MV\cdot cm^{-1}$, the maximum theoretical mobility of electron is 2000 $cm^2\cdot V^{-1}\cdot s^{-1}$ [7]. The competitive advantages of GaN devices are presented in [8]. GaN is considered a good alternative for all devices that need fast carrier transport or a high breakdown voltage.

GaN has been utilized to create a variety of devices, including Metal-Semiconductor FETs and MOSFET based on GaN. The structure shown in Fig. 1 has a buried channel with fewer defects. HFET can be called as modulation-doped FET (MODFET).

MODFET is an HFET in which the undoped channel acquires carriers by the doping of one layer so that the channel becomes conductive, which is commonly called a Two-Dimensional Electron Gas (2DEG). Band bending occurs due to bandgap discontinuity and the doping that determines Fermi level. Thus, the conductive channel is frequently restricted in a quantum well. However, because the channel contains no dopant, the scattering effect is completely eliminated. Therefore, the electron mobility becomes high. On the other hand, the gate is located away from the channel and thus results in low gate control [9].

Despite the many benefits provided by GaN high electron mobility transistors (HEMTs), these transistors suffer from a number of issues. First off, there is typically a significant concentration of bulk and surface defects in the epitaxial layers of GaN employed in HFETs. There may be dangling bonds and dislocations among these defects on the barrier. Charges trapped by these defects may generate Coulomb scattering in the channel, even while 2DEG is buried. Furthermore, the cut-off frequency may degrade, which affects the high-frequency performance [10, 11]. Moreover, at high-power and high-frequency levels, this condition can cause major degradation issues [12]. Second, this structure generates a large gate-leakage current.

In contrast to that of the MOSFET structure, gate dielectric is absent, which causes a negative effect on the gate-current-leakage levels. Compared with an ideal Schottky gate device, the Schottky gate-leakage current in AlGaN/GaN HEMT is significantly higher [13, 14]. Thus, a metal–oxide–semiconductor HEMT (MOSHEMT) device can solve the problems suffered by the HEMT device [15 ,16].

In the present work, a characterization and simulation study are performed to provide the best design of GaN-based HEMTs using Synopsys® Sentaurus TCAD. Simulation is performed to improve the cutoff frequency. The effect of the AlGaN layer thickness, gate length, Al mole fraction, and concentration level of the interface traps on the electrical performance of the device is discussed.

This paper is organized as follow: Section II presents device description of AlGaN/GaN MOSHEMT, Section III introduces the device calibration, section IV describes the results and discussion, Section V provide the conclusion of the paper.

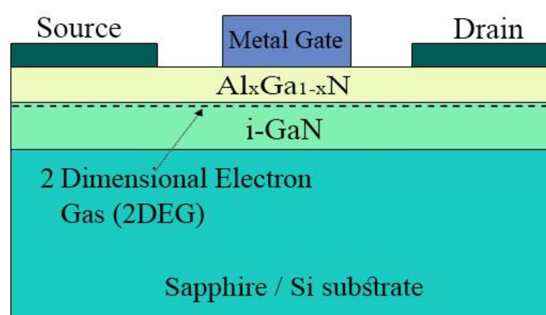

Figure. 1 Illustration of a typical HFET structure [9].

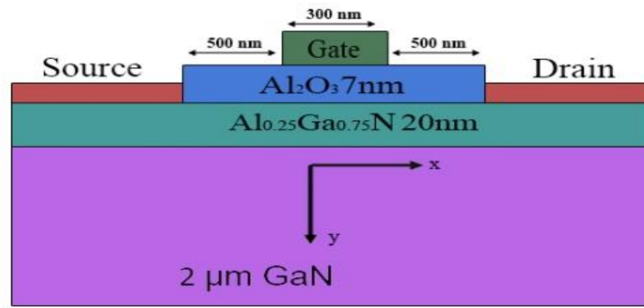

Figure 2 Structure used in the simulation [9].

II. DEVICE DESCRIPTION

The structure used in our simulation is shown in Fig. 2 [9]. The coordinate system shown in Fig. 2 is the x-y axis, where the AlGaN/GaN contact is located on the y = 0 line. The device center is shown by the line at x = 0. Both the distances between the source-gate and the drain-gate are set at 500 nm. The drain and source regions are characterized by an ohmic contact with a highly n-doped concentration of $1\times10^{20}/cm^{-3}$. The gate length is equal to 300 nm with a workfunction of 4.4 eV. The AlGaN/GaN MOSHEMT structure consists of a 20-nm AlGaN barrier followed by GaN layer with a thickness of 2 µm. The presence the heterostructure of AlGaN/GaN benefits the formation of 2DEG along the AlGaN/GaN interface [17, 18]. Formation of 2DEG occurs in the lower bandgap GaN layer at the interface. The layer of GaN is n-type doped with a concentration of 1×10^{16} cm^{-3}. The gate dielectric used in the simulation is Al_2O_3 with a bandgap of 8.7 eV and high dielectric constant value of nine. The gate dielectric thickness is 7 nm [19]. The effect of the polarization in the AlGaN/GaN heterostructure is a key factor in the 2DEG formation [9]. In all structure interfaces, the polarization charge is computed according to [20]. The interfaces between the high-k dielectric and the AlGaN layer and between the AlGaN and GaN layers have the biggest effects on the density of the 2DEG, as shown in Fig. 3. It is expected that the GaN layer is completely relaxed with just spontaneous polarization (P_{SP}) because it is substantially thicker than the AlGaN layer. P_{SP} effect is the name given to the polarization phenomenon brought on by the noncentral-symmetric structure in GaN. P_{SP} effect similarly occurs in AlGaN, which has a different magnitude from that of GaN. The difference in the P_{SP} of GaN and AlGaN is one cause of 2DEG. When layers are joined at the heterojunction interface, the strain or stress on the crystal lattice caused by physical distortion leads to piezoelectric polarization (P_{PE}).

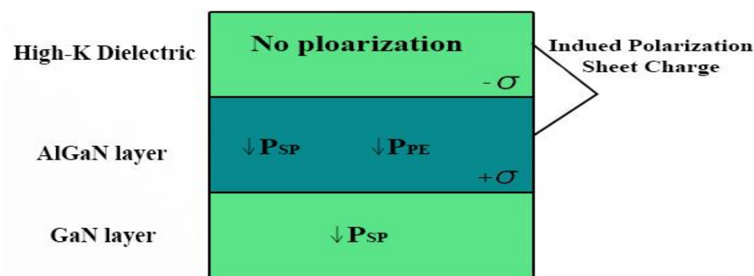

Figure 3 Polarization of the interfaces and the respective induced-polarization charges.

The charge density caused by polarization can be characterized by the following:

$$\sigma(P_{SP}+P_{PE}) = -(P_{\text{top}}-P_{\text{bottom}}) = P_{\text{bottom}}-P_{\text{top}} \qquad (1)$$

P stands for total polarization (i.e. spontaneous, SP, and piezoelectric, PE,), where P_{top} (polarization in the layer of AlGaN) and P_{bottom} (polarization in the layer of GaN). To determine the value of the induced bound charge sheet, divide equation (1) by the electric charge, q.

Severe crystal defects in structure result from the immaturity of III-nitride technology and the lattice mismatch between AlGaN and GaN [6]. These structure defects can effectively turn into traps. Additionally discovered as a potential source of carriers for 2DEG are donor-like surface states [21]. Therefore, an accurate evaluation of the trap concentration is necessary to guarantee a precise simulation.

The bulk trap density in most III-nitride materials is in the range of 10^{15}–10^{18} cm^{-3} in several studies such as [22] and [23]. Meanwhile, the density of the bulk trap of the GaN and AlGaN in this simulation is changed to 5×10^{17} cm^{-3}. Based on the mean of the values derived from the literature [22–24] these traps have been described as acceptor-like since they are located at 1 eV above the midgap. According to [21], the interface states directly affect 2DEG. At the AlGaN/GaN contact, it is assumed that there are no traps. In view of this, the AlGaN and high-k dielectric interface is where the majority of interface traps are located. In this study, the interface state-density concentration is 3.0×10^{13} $cm^{-2}\cdot eV^{-1}$ and is a donor-like (0.2 eV above the midgap of AlGaN) trap, as presented in [21]. Using surface passivation, the interface state in the range 10^{10}–10^{11} $cm^{-2}\cdot eV^{-1}$ level, according to [25].

III. DEVICE CALIBRATION

Before caliberation of the HFET structure shown in Fig. 2 is performed using TCAD Sentaurus. Four models for mobility are used in the simulation, which include the Masetti (doping-dependent mobility), constant-mobility, Canali (high-field-saturation mobility), and Lombardi (interface-degradation mobility) models [9]. The default parameters were used in the TCAD simulation is follows: mole fraction in AlGaN layer is 25%, thickness of AlGaN is 20 nm, and dielectric constant is 9.8, electron Mobility is 1200 [cm^2/Vs], bandgap of GaN is 3.4 [eV].

The simulation results are calibrated based on the experimental measurements in [9, 26]. Fig. 4 shows the I_{DS}–V_{DS} characteristics at V_{GS}=0 V, whereas Fig. 5 shows I_{DS}–V_{GS} at V_{DS}=0.5 V with the measurement data. The simulated results agree well with the measurement data.

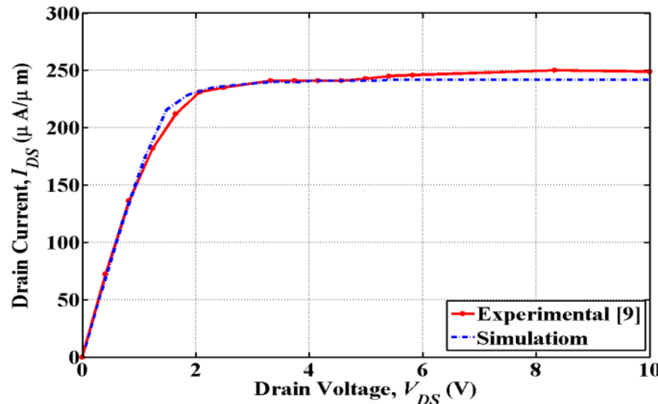

Figure 4 Calibrated I_{DS}–V_{DS} characteristics of AlGaN/GaN MOSHEMT [9].

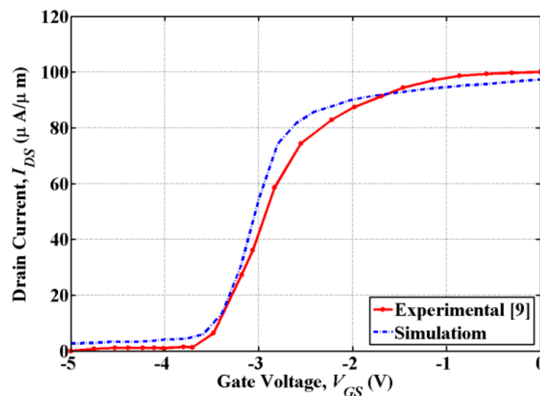

Figure 5 Calibrated I_{DS}–V_{GS} characteristics of AlGaN/GaN MOSHEMT [9].

IV. RESULTS AND DISCUSSION

The simulation is divided into two analysis sections: geometrical- and technological-parameter analyses.

A. *Geometrical Parameters Analysis*

To be acceptable in high-fast and large-power applications, the cutoff frequency f_t determines the RF achievement of any transistor design [27,28]. The structure shown in Fig. 2 is used without change, while the thickness of the AlGaN barrier-layer and gate length are scaled.

The relationship between g_m and f_t is important for improving the cutoff frequency. Transconductance is defined as the differentiation of the drain current with respect to the gate voltage at a constant drain voltage. The electron velocity and charge density at the contact rise as the electric field increases, leading in improved g_m. The device sensitivity is enhanced by high drain current, strong carrier concentration, and good transconductance. A high transconductance rating indicates that the device is fast and has a high drain current. The capacitance total is calculated as follows:

$$C_{gg}=C_{gd}+C_{gs} \quad (2)$$

The capacitance between the gate and drain is indicated as C_{gd}, whereas that between the gate and source is indicated as C_{gs}. C_{gg} affects the power dissipation and switching behavior. C_{gg} and g_m influence the cut-off frequency. Cut-off frequency f_t is inversely proportional to gate capacitance C_{gg} [29]. To improve the high-frequency performance of HEMTs, smaller values of C_{gs} and C_{gd} are required. f_t can be calculated as follows:

$$f_t = \frac{g_m}{2\pi\left(C_{gs}+C_{gd}\right)} \quad (3)$$

1) *Varying AlGaN barrier layer thickness, (t_{AlGaN})*

Barrier-layer thickness t_{AlGaN} is varied from 10 to 40 nm. Fig. 6 shows the I_{DS}–V_{DS} characteristics at different t_{AlGaN} values. With an increase in t_{AlGaN}, the 2DEG density rises, resulting in larger drain current I_{DS}. Fig. 7 shows cut-off frequency f_t at different t_{AlGaN} values. Clearly, f_t increases with t_{AlGaN} up to its maximum value of 20 nm. Then, it begins to decrease. This result can be explained by the cut-off frequency f_t behaviour is defined by gm, C_{gs}+C_{gd}; C_{gs}+C_{gd} decreases as t_{AlGaN} increases [30], whereas the gm behaviour results from behaviour of the 2DEG in the channel.

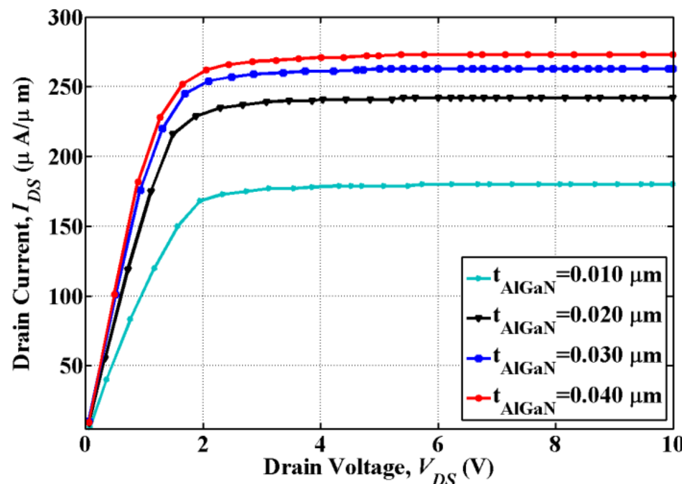

Figure 6 I_{DS}–V_{DS} characteristics at different t_{AlGaN} values

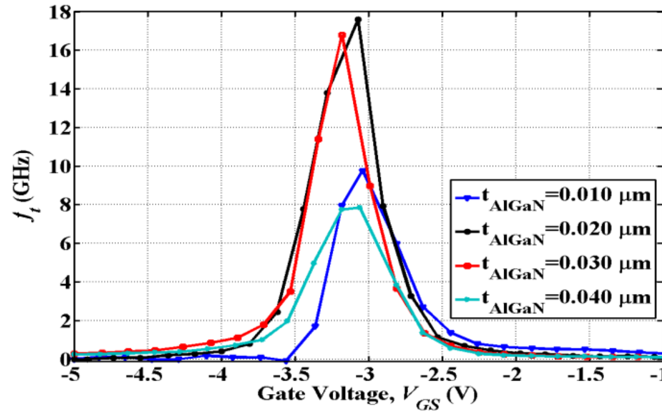

Figure 7 f_t versus V_{GS} at different t_{AlGaN} values.

2) Varying Gate Length, Lg

Gate length L_g is changed from 400 to 80 nm. The effects of L_g variation on I_{DS}, g_m, and f_t are shown in Fig. 8 to Fig. 10, respectively. Fig. 8 shows that I_{DS} increases with the decrease L_g [31]. Fig. 9 clearly shows that decreasing the L_g results in an increase in f_t up to its maximum value of 45.7 GHz at L_g=100 nm, then, the frequency begins to decrease. For the transconductance g_m as shown in Fig. 10, it follows the frequency behavior with the gate length, increasing to maximum at Lg=100nm then decreasing. Two factors limiting the frequency performance, short channel effects and parasitic capacitance [32]. Furthermore, because f_t is inversely related to the gate capacitance, a reduction in the gate length results in a significant reduction in the gate capacitance, which leads to a significant improvement in the AC characteristics.

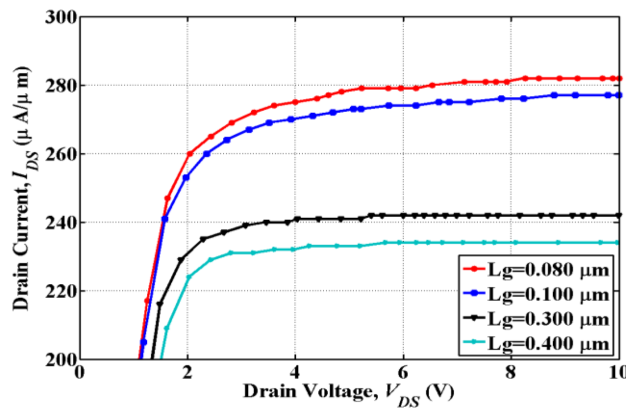

Figure 8 I_{DS}-V_{DS} characteristics for different gate length.

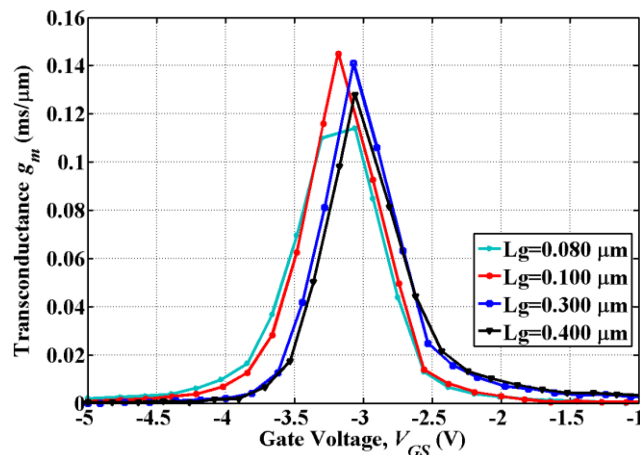

Figure 9 g_m–V_{GS} at different Lg values.

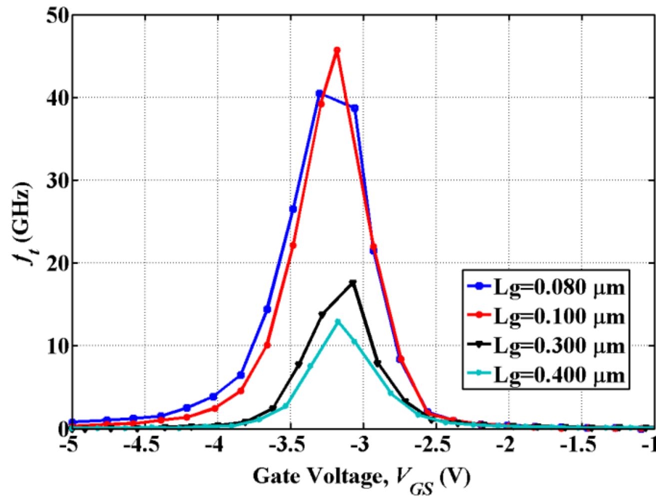

Figure. 10 f_t versus V_{GS} at different Lg values.

B. Technological Parameters Analysis

This section presents the effect of changing both the Al mole fraction of $Al_xGa_{1-x}N$ and acceptor-like traps in the $AlGaN/Al_2O_3$ interface $AlGaN/Al_2O_3$ interface.

1) Impact of Al mole fraction (x) in AlxGa1-xN

The Al mole fraction is varied between 25% and 40%. The AlGaN barrier-layer thickness is 20 nm. Fig. 11 shows the change in I_{DS} due to the $Al_xGa_{1-x}N$ modification. The electron density in 2DEG increases as mole fraction x increases, resulting in larger drain current I_{DS}. We can deduce that as the 2DEG density increases, transconductance g_m increases and consequently [33], the cut-off frequency. The polarization-induced electric field increases as the Aluminium mole fraction rises. Accordingly, the junction conduction band and electron confinement increase, but the electron scattering from 2DEG into the GaN buffer decreases [32]. Thus, the short-channel effects are reduced, and output resistance RDS increases [34].

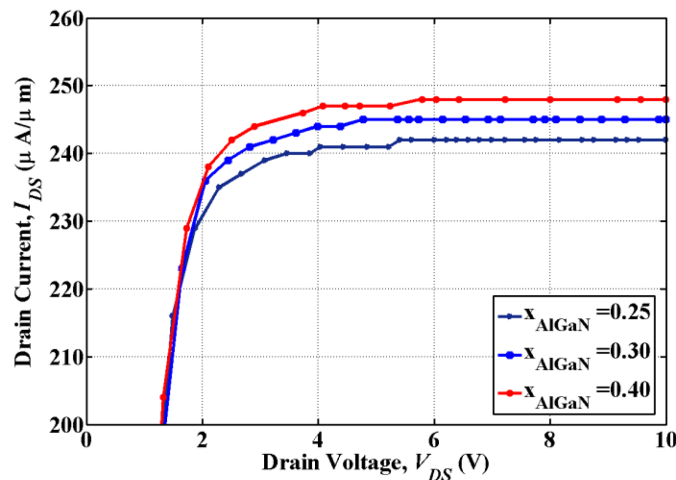

Figure 11 I_{DS}–V_{DS} characteristics at different x_{AlGaN} values.

2) The effect of the concentration level of the interface traps

At the interface of the Al_2O_3/AlGaN, both acceptor- and donor-like traps exist. A passivation procedure is used to decrease the acceptor-like traps, as presented in [9]. We use both types of traps at the interface in our simulation. The simulations are done tow times, the first one is performed without acceptor-like trap while the second used acceptor-like traps of 1×10^{12} $cm^{-2}\cdot eV^{-1}$. At this interface the donor-like trap is constant at 3×10^{13} $cm^{-2}\cdot eV^{-1}$. The I_{DS}–V_{DS} characteristics shown in Fig. 12 exhibits results close to the results presented in [9].

A reduction in the traps results in an increase in the drive current as confirmed by results of the simulation shown in Fig. 12. In order to improve the RF performance of many GaN HEMTs, many studies have been carried out. A comparison of various HEMT devices is listed in Table II.

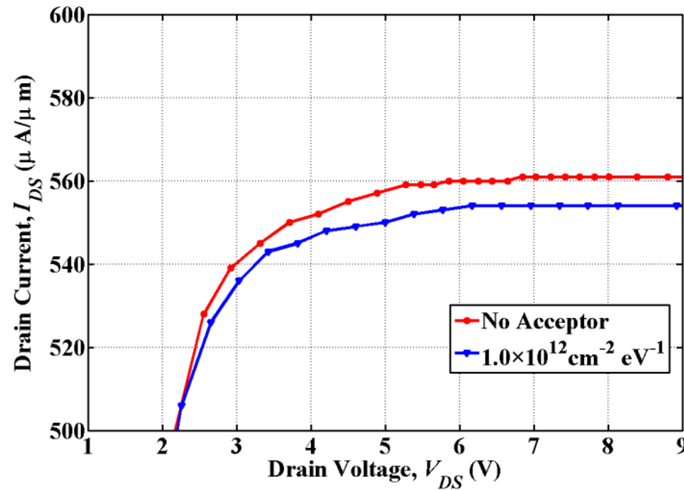

Figure 12 I_{DS}–V_{DS} characteristics.

Table II f_t frequency different HEMT devices comparison

Reference	Lg (nm)	HEMT device	f_t (GHz)
2020 [35]	600	AlGaN/GaN HEMT	24.4
2020 [36]	-	GaN/GaN/AlGaN on SiC	28
2020 [19]	250	AlGaN/GaN Based DG MOSHEMT	19.25
2021 [37]	800	AlGaN/GaN HEMT	14.9
2021 [29]	100	Dual Gate AlGaN/GaN HEMT	11
This work	100	AlGaN/GaN based MOSHEMT	**45.7**

V. CONCLUSION

In this study, an AlGaN/GaN MOSHEMT is calibrated and studied using the Sentaurus TCAD tool. The simulation of AlGaN/GaN is performed according to two groups: geometrical- and technological-parameter analyses. The geometrical-parameter analysis includes the variation in the AlGaN barrier-layer thickness and gate length, whereas the technological-parameter analysis involves changing the Aluminium mole fraction of $Al_xGa_{1-x}N$, and acceptor-like traps between Al_2O_3 and AlGaN interface. The simulation results demonstrate that the drain current increases with the reduction in the gate length to 80 nm, and increases the Aluminium-mole fraction to 40% and the AlGaN barrier-layer thickness to 40 nm. In the absence of acceptor-like traps between Al_2O_3 and AlGaN interface, the drain current reaches 567 (μA/μm). Meanwhile, the cut-off frequency improves with the increase in the thickness of the AlGaN layer to 20 nm at 17.6 GHz. The reduction in the gate length to 100 nm occurs at 45.7 GHz. Finally, the transconductance is 145 at a 100-nm gate length. These results indicate that the AlGaN/GaN MOSHEMT is an outstanding candidate for high-frequency application.

REFERENCES

[1] P. Pal, Y. Pratap, M. Gupta, S. Kabra, and H. D. Sehgal, "Performance analysis of ScAlN/GaN high electron mobility transistor (HEMT) for biosensing application," in Proc. of 2020 5th International Conference on Devices, Circuits and Systems (ICDCS), Coimbatore, India, pp. 203-206, 2020.

[2] JADLI, Utkarsh, et al., "Modeling Power GaN-HEMTs Using Standard MOSFET Equations and Parameters in SPICE," Electronics, 10.2: 130, 2021.

[3] M. A. Alim, C. Gaquiere, and G. Crupi, “An experimental and systematic insight into the temperature sensitivity for a 0.15-μm gate-length HEMT based on the GaN technology,” Micromachines, vol. 12, no.5,2021, https://doi.org/10.3390/mi12050549

[4] O. Ambacher, J. Smart, J.R. Shealy, N.G. Weimann, K. Chu, M. Murphy, W.J Schaff, L.F. Eastman, R. Dimitrov, L. Wittmer & M. Stutzmann, “Two-dimensional electron gases induced by spontaneous and piezoelectric polarization charges in N- and Ga-face AlGaN/GaN heterostructures,” Journal of applied physics, Vol. 85, pp.3222-3233,1999.

[5] S.J. Pearton, F. Ren, A.P. Zhang & K.P. Lee, “Fabrication and performance of GaN electronic devices,” Materials Science and Engineering, Vol. 30, pp.55-212, 2000

[6] R. Szweda, “Gallium Nitride and Related Wide Bandgap Materials and Devices: A Market and Technology Overview 1998-2003,” 2nd ed., Elsevier Advanced technology, 2000.

[7] P. Joachim, “Nitride Semiconductor Devices: Principles and Simulation,” John Wiley & Sons, 2007.

[8] U.K. Mishra, P. Parikh & Y.F. Wu, “AlGaN/GaN HEMTs - An Overview of Device Operation and Applications”, Proceedings of the IEEE, Vol. 90, , pp.1022-1022, 2002.

[9] L.K. Edwin, “Characterization and Numerical Simulation of Gallium Nitride-Based Metal-Oxide-Semiconductor High Electron Mobility Transistor with High-K Gate Stack,” M.E. Thesis, National University of Singapore, 2012.

[10] F.A. Marino, N. Faralli, T. Palacios, D.K. Ferry, S.M. Goodnick & M. Saraniti, “Effects of Threading Dislocations on AlGaN/GaN High-Electron Mobility Transistors,” IEEE transactions on Electron Devices, Vol. 57, pp.353-360, 2009.

[11] G.H. Jessen, R.C. Fitch, J.K. Gillespie, G.D. Via, B.D. White, S.T. Bradley, D.E. Walker & L.J. Brillson, “Effects of deep-level defects on ohmic contact and frequency performance of AlGaN/GaN high-electron-mobility transistors,” Applied physics letters, Vol. 85, pp.485-485, 2003.

[12] W. Saito, M. Kuraguchi, Y. Takada, K. Tsuda, I. Omura & T. Ogura, “Influence of surface defect charge at AlGaN-GaN-HEMT upon Schottky gate leakage current and breakdown voltage,” IEEE Transactions on Electron Devices, Vol. 52, pp.159-159, 2005.

[13] W. Saito, Y. Takada, M. Kuraguchi, K. Tsuda, I. Omura & T. Ogura, “600V AlGaN/GaN power-HEMT: Design, fabrication and demonstration on high voltage DC-DC converter,” IEEE International Electron Devices Meeting, pp.23-7, 2003

[14] W. Saito, M. Kuraguchi, Y. Takada, K.; Tsuda, I. Omura & T. Ogura, “High breakdown voltage undoped AlGaN-GaN power HEMT on sapphire substrate and its demonstration for DC-DC converter application,” IEEE Transactions on Electron Devices, Vol. 51, pp.1913-1913, 2004.

[15] Huang, Cheng-Yu, et al. “Improved Electrical Characteristics of AlGaN/GaN High-Electron-Mobility Transistor with Al2O3/ZrO2 Stacked Gate Dielectrics,” Materials 15.19 (2022): 6895.

[16] Lin, Yu-Shyan, and Chi-Che Lu. "AlGaN/GaN Metal Oxide Semiconductor High-Electron Mobility Transistors with Annealed TiO2 as Passivation and Dielectric Layers." Micromachines 14.6 (2023): 1183.

[17] I. Nifa, C. Leroux, A. Torres, M. Charles, D.; Blachier, G. Reimbold, G. Ghibaudo & E. Bano, “Characterization of 2DEG in AlGaN/GaN heterostructure by Hall effect,” Microelectronic Engineering, Vol. 178, pp.128-131, 2017.

[18] I. Nifa, C. Leroux, A. Torres, M. Charles, G. Reimbold, G. Ghibaudo & E. Bano, “Characterization and modeling of 2DEG mobility in AlGaN/AlN/GaN MIS-HEMT,” Microelectronic Engineering, Vol. 215, 110976, 2019.

[19] M. Verma & A. Nandi, “Design and Analysis of AlGaN/GaN Based DG MOSHEMT for High-Frequency Application,” Transactions on Electrical and Electronic Materials, Vol. 2, pp. 427-43, 2020.

[20] C. Wood & D. Jena, “Polarization effects in semiconductors: from ab initio theory to device applications,” Springer Science & Business Media, 2007.

[21] J.P. Ibbetson, P.T. Fini, K.D. Ness, S.P. DenBaars, J.S. Speck & U.K. Mishra, “Polarization effects, surface states, and the source of electrons in AlGaN/GaN heterostructure field effect transistors,” Applied Physics Letters, Vol. 77, pp.250-252, 2000.

[22] D.C. Look, Z.Q. Fang & B. Claflin, “Identification of donors, acceptors, and traps in bulk-like HVPE GaN,” Journal of crystal growth, Vol. 281, , pp.143-150, 2005.

[23] S. Xie, J. Yin, S. Zhang, B. Liu, W. Zhou & Z. Feng, “Trap behaviors in AlGaN–GaN heterostructures by C–V characterization,” Solid-state electronics, Vol. 53, pp.1183-1185, 2009.

[24] A. Brannick, N.A. Zakhleniuk, B.K. Ridley, L.F. Eastman, J.R. Shealy & W.J. Schaff, “Hydrodynamic simulation of surface traps in the AlGaN/GaN HEMT,” Microelectronics Journal, Vol. 40, pp.410-412, 2009.

[25] X., Liu, H.C., Chin, L.S. Tan & Y.C. Yeo, “In situ Surface Passivation of Gallium Nitride for Metal–Organic Chemical Vapor Deposition of High-Permittivity Gate Dielectric,” IEEE transactions on electron devices, Vol. 58, pp.95-102, 2010.

[26] X. Liu, B. Liu, E. K. F. Low, H.-C. Chin, W. Liu, M. Yang, L. S. Tan & Y.-C. Yeo, “Diamond-like carbon (DLC) liner with highly compressive stress formed on AlGaN/GaN MOS-HEMTs with in situ silane surface passivation for performance enhancement,” IEEE International Electron Device Meeting, San Francisco CA, Dec. 6 - 8, 2010, pp.11.3.1 - 11.3.4. 2010.

[27] N. Islam, M. F. P. Mohamed, M. F. A. J. Khan, et al., “Reliability, applications and challenges of GaN HEMT technology for modern power devices: A review,” Crystals, vol. 12, no. 11, 2022, https://doi.org/ 10.3390/cryst12111581

[28] W. A. Jabbar, A. Mahmood, and J. Sultan, “Modeling and characterization of optimal nano-scale channel dimensions for fin field effect transistor based on constituent semiconductor materials,” TELKOMNIKA Telecommunication Computing Electronics and Control, vol. 20, no. 1, pp. 221-234, 2022.

[29] M., Rao, R., Ranjan, N., Kashyap & R.K. Sarin, “Performance Analysis of Normally-on Dual Gate Algan/Gan Hemt,” Transactions on Electrical and Electronic Materials, pp.1-9, 2021.

[30] A. Vais, Physical simulation of GaN based HEMT”, M.E. Thesis, Chalmers University of Technology Gothenburg, Sweden, 2012.

[31] Abdkadir, F. Natheer, et al. “Enhancement Performance of High Electron Mobility Transistor (HEMT) Based on Dimensions Downscaling,” International Journal of Electrical and Electronic Engineering & Telecommunications. IJEETC, 2023.

[32] S. Lei, W. C Cheng, J. Wu, L. Wang, Q. Wang, G. Xia, & H. Yu, “Low leakage GaN HEMTs with sub-100 nm T-shape gates fabricated by a low-damage etching process,” Journal of Materials Science: Materials in Electronics, Vol. 31(8), pp.5886-5891,2020

[33] J. Ajayan, D. Nirmal, P. Mohankumar, et al., “Challenges in material processing and reliability issues in AlGaN/GaN HEMTs on silicon wafers for future RF power electronics & switching applications: A critical review,” Materials Science in Semiconductor Processing, vol. 151, #106982, Nov. 2022.

[34] T. Palacios, Y. Dora, A. Chakraborty, C. Sanabria, S. Keller, S.P. DenBaars & U.K. Mishra, “Optimization of AlGaN/GaN HEMTs for high frequency operation,” Physica Status Solidi (a), Vol. 203, pp.1845-1850, 2006.

[35] Huang, Chong-Rong, et al., “The characteristics of 6-inch GaN on Si RF HEMT with high isolation composited buffer layer design,” Electronics 10.1 (2020): 46.

[36] A.S. Augustine, D. Nirmal, L. Arivazhagan, J. Ajayan & A. Varghese, “Enhancement of Johnson figure of merit in III-V HEMT combined with discrete field plate and AlGaN blocking layer,” International Journal of RF and Microwave Computer-Aided Engineering, Vol. 30, 22040, 2020.

[37] Huang, Zhihui, et al. "Novel gate air cavity GaN HEMTs design for improved RF and DC performance,” Results in Physics 29 (2021): 104718.